Electron paramagnetic resonance and optical spectroscopy of Yb^{3+} ions in SrF_2 and BaF_2; an analysis of distortions of the crystal lattice near Yb^{3+}

2003 J. Phys.: Condens. Matter 15 2833

(http://iopscience.iop.org/0953-8984/15/17/332)

INSTITUTE OF PHYSICS PUBLISHING JOURNAL OF PHYSICS: CONDENSED MATTER

J. Phys.: Condens. Matter **15** (2003) 2833–2847 PII: S0953-8984(03)57592-0

Electron paramagnetic resonance and optical spectroscopy of Yb^{3+} ions in SrF_2 and BaF_2; an analysis of distortions of the crystal lattice near Yb^{3+}

M L Falin[1], K I Gerasimov[1], V A Latypov[1] and A M Leushin[2]

[1] Zavoisky Physical-Technical Institute, Kazan 420029, Russia
[2] Kazan State University, Kazan 420008, Russia

E-mail: falin@kfti.knc.ru

Received 18 December 2002
Published 22 April 2003
Online at stacks.iop.org/JPhysCM/15/2833

Abstract

SrF_2 and BaF_2 crystals, doped with the Yb^{3+} ions, have been investigated by electron paramagnetic resonance and optical spectroscopy. As-grown crystals of SrF_2 and BaF_2 show the two paramagnetic centres for the cubic (T_c) and trigonal (T_4) symmetries of the Yb^{3+} ions. Empirical diagrams of the energy levels were established and the potentials of the crystal field were determined. Information was obtained on the SrF_2 and BaF_2 phonon spectra from the electron-vibrational structure of the optical spectra. The crystal field parameters were used to analyse the crystal lattice distortions in the vicinity of the impurity ion and the F^- ion compensating for the excess positive charge in T_4. Within the frames of a superposition model, it is shown that three F^- ions from the nearest surrounding cube, located symmetrically with respect to the C_3 axis from the side of the ion-compensator, approach the impurity ion and cling to the axis of the centre when forming T_4. The F^- ion located on the axis of the centre between the Yb^{3+} ion and ion-compensator, also approaches close to the impurity ion.

1. Introduction

Crystals with fluorite structure MeF_2 (where Me is Cd, Ca, Sr, Pb, Ba), doped with rare-earth ions, are of interest due to the fact that, on the one hand, they find wide use (laser working media, scintillation materials, superionic conductors etc) and, on the other hand, they are convenient model systems for studying the magneto-optical properties of impurity paramagnetic ions. The Yb^{3+} ion has the most simple energy level diagram compared with other rare-earth ions. It consists of the $^2F_{7/2}$ ground level and the $^2F_{5/2}$ excited level, 10^4 cm^{-1} away from the ground level. This feature of the ytterbium ion makes it attractive for investigations of optical properties.

In the fluorite homological series, the Yb^{3+} ions were best investigated in CaF_2 (by electron paramagnetic resonance (EPR), electron–nuclear double-resonance (ENDOR) and optical spectroscopy). However, complicated absorption and luminescence spectra and, accordingly, the complicated Stark structure of a large number of paramagnetic centres (PCs) formed in this crystal, have not been unambiguously interpreted up to now [1–4]. At the same time, the optical data for the Yb^{3+} ions in other MeF_2 crystals are practically absent. Unlike CaF_2, these crystals are not multi-central, which simplifies the identification of optical spectral lines. For example, the Yb^{3+} ions in SrF_2 and BaF_2 form only two PCs during the crystal growth: of cubic (T_c) and trigonal (T_4) symmetries [4]. In the latter case, the compensation for the excess positive charge occurs with the additional ion of fluorine in the centre of the free cube nearest to the Yb^{3+} ion along the C_3 axis. By means of thermal processing (hydrolysis), these centres are partly transformed to PCs of trigonal symmetry T_2, where the oxygen ion replaces one of the fluorine ions in the nearest cubic surrounding of Yb^{3+} [2]. So, the number of the PCs in SrF_2 and BaF_2 can be increased up to 3. Since this process is controlled, the additional way appears to identify the optical spectral lines.

Previously we investigated the Yb^{3+} ion in PbF_2 (T_c) [5] and SrF_2 (T_2) [6]. This work presents the results of the further EPR and optical investigations of the Yb^{3+} ion forming T_c and T_4 PCs in SrF_2 and BaF_2 crystals.

2. Experimental results

The SrF_2 (BaF_2) crystals were grown by the Bridgman–Stockbarger method in graphite crucibles in a fluorine atmosphere. We used crystals with ytterbium concentrations of 0.05, 0.1, 0.2, 0.5, 1% for SrF_2 and 0.01, 0.05, 0.1, 0.2% for BaF_2. The measurements were carried out on a modified ERS-231 spectrometer (Berlin, Centre for Scientific Instruments) [7] at $T = 4.2$ K. Optical spectra at $T = 2$, 77 and 300 K and magnetic circular dichroism (MCD) spectra at $T = 2$ K were recorded on a home-made multifunctional spectrometer [8]. The luminescence of the crystals was excited by the light of a xenon lamp (power 1 kW), passing through a red glass filter. Luminescence excitation spectra were corrected on the spectrum of the lamp radiation. A semiconductor laser diode ATC-C1 000-100-TMF-965 (St Petersburg) of 1 W was used as a source of a laser selective excitation (LSE) with laser linewidth of the order of 2 nm and the laser emission wavelength tunable from 963 nm (10 381 cm^{-1}) to 969 nm (10 317 cm^{-1}).

The angular dependences of the EPR spectra on a magnetic field H rotated in the (110) plane show the presence of two Yb^{3+} PCs of different symmetry, T_c and T_4, in all SrF_2 and BaF_2 crystals used in this work. The EPR spectra of these centres are well known and consequently not given here. The values of the spin Hamiltonian parameters (g-factors and the hyperfine constants) for the PCs obtained in our EPR experiments coincided with those published in [1–4]. Therefore we give the literature data in the tables below.

Figure 1 (B) and (A) show the spectra of the luminescence and luminescence excitation, respectively, in SrF_2 crystals with Yb^{3+} concentration $c = 0.05\%$ at $T = 2$ K; (C) and (D) show the corresponding spectra for BaF_2 crystals with Yb^{3+} concentration $c = 0.01\%$. Arrows with a numbered labels show the spectral lines supposedly corresponding to T_c and T_4. These marks correspond to those of optical transitions in the diagrams of energy levels in figure 1 (inset). Since at $T = 2$ K there are no spectral lines in the luminescence spectra at the frequencies higher than 10 360 cm^{-1} or the luminescence excitation spectra at the frequencies lower than 10 180 cm^{-1}, these regions are not shown in figure 1. As one can see from these spectra, the number of the lines observed exceeds the number of electron transitions predicted for T_c and T_4 from symmetry considerations. This is due to the fact that the Yb^{3+} ion optical spectra

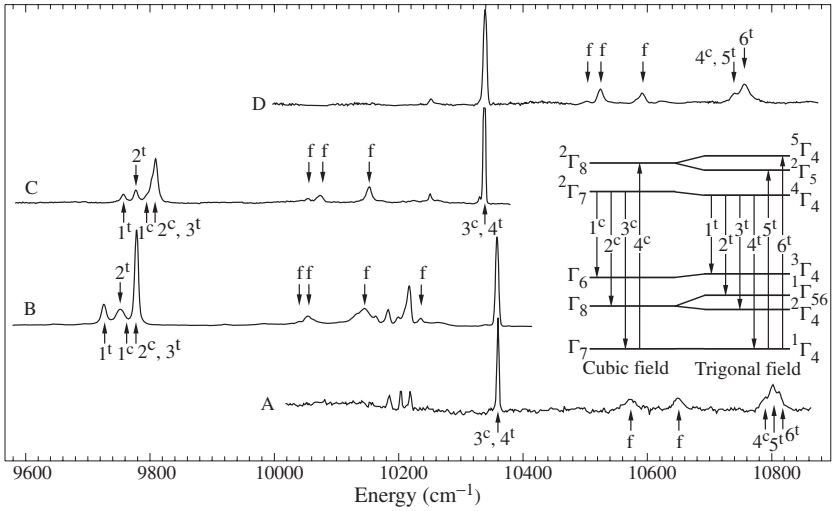

Figure 1. Luminescence (B, C) and luminescence excitation (A, D) spectra of Yb^{3+} ($c = 0.05\%$) in SrF_2 (A, B) and Yb^{3+} ($c = 0.01\%$) in BaF_2 (C, D) at $T = 2$ K. Here and in figures 2–5, numbering of spectral lines corresponds to the numbering of transitions in the inset. Arrows with a symbol 'f' denote the electron-vibrational transitions.

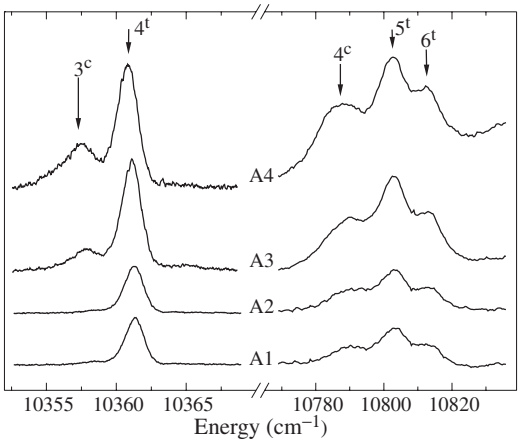

Figure 2. Fragments of the luminescence excitation spectra in the SrF_2:Yb^{3+} with Yb^{3+} concentrations equal to 0.05% (A1), 0.01% (A2), 0.2% (A3) and 0.5% (A4) at $T = 2$ K.

always have a distinct electron-vibrational character and some of the lines are the phonon satellites of purely electron transitions. The arrows with symbol 'f' in figure 1 designate the most intensive electron-vibrational transitions. Table 1 shows the phonon frequencies in the observed electron-vibrational spectra of the luminescence excitation and luminescence.

Figures 2 and 3 show the fragments of the luminescence excitation spectra for different concentrations of the Yb^{3+} ion in SrF_2 and BaF_2 crystals, respectively. These spectra are measured with resolution of about 3 cm^{-1}. In the region of 10 360 cm^{-1} two narrow and sufficiently intensive lines with frequencies of 10 358 and 10 361 cm^{-1} are observed in the luminescence excitation and luminescence spectra of the SrF_2:Yb^{3+} crystal at 2 K. To attribute optical spectral lines to T_c and T_4 the following method was used. The concentration

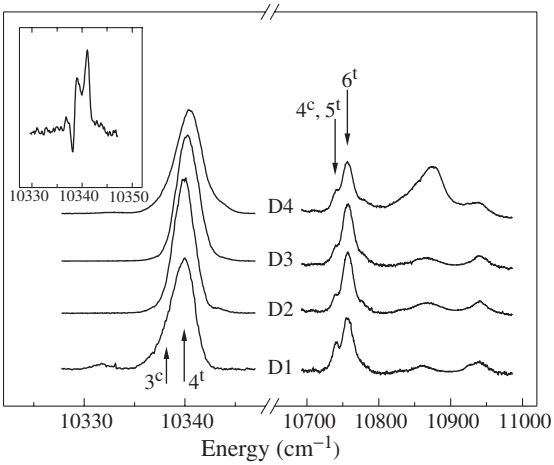

Figure 3. Fragments of the luminescence excitation spectra in the BaF_2:Yb^{3+} with Yb^{3+} concentrations equal to 0.01% (D1), 0.05% (D2), 0.1% (D3) and 0.2% (D4) at $T = 2$ K. In the inset, the fragment of the MCD spectrum in BaF_2:Yb^{3+}($c = 0.2\%$) at $H = 300$ mT and $T = 2$ K is shown.

Table 1. Phonon frequencies in the luminescence excitation and luminescence spectra of T_c and T_4 in SrF_2 and BaF_2.

Crystal	Temperature (K)	Electron transitions	Phonon frequencies (cm^{-1})	Satellite type
SrF_2	2	$^1\Gamma_7 \rightarrow {}^2\Gamma_8$	112; 206	Anti-Stokes
		$^1\Gamma_7 \rightarrow {}^2\Gamma_7$	96; 208; 290	Anti-Stokes
		$^2\Gamma_7 \rightarrow {}^1\Gamma_8$	161	Stokes
		$^2\Gamma_7 \rightarrow {}^1\Gamma_7$	84; 175	Stokes
	300	$^2\Gamma_7 \rightarrow {}^1\Gamma_7$	94; 207; 291	Anti-Stokes
			203; 297	Stokes
BaF_2	2	$^1\Gamma_7 \rightarrow {}^2\Gamma_8$	95; 185; 254; 324	Anti-Stokes
		$^1\Gamma_7 \rightarrow {}^2\Gamma_7$	113; 183; 281	Anti-Stokes
		$^2\Gamma_7 \rightarrow {}^1\Gamma_8$	114; 184; 262	Stokes
		$^2\Gamma_7 \rightarrow {}^1\Gamma_7$	89; 188; 266; 336	Stokes
	300	$^2\Gamma_7 \rightarrow {}^1\Gamma_7$	78; 182; 259	Anti-Stokes
			78; 174; 262	Stokes

dependences of the intensity ratios of the optical lines were compared with the analogous dependences of the EPR lines of the even Yb^{3+} isotopes of T_c and T_4. To this end we measured the EPR spectra of the crystals SrF_2:Yb^{3+} ($c = 0.05, 0.1, 0.2, 0.5\%$) and BaF_2:Yb^{3+} ($c = 0.01$, 0.05, 0.1, 0.2%) for $H \parallel [111]$. The qualitative dependences of the EPR intensity ratios of T_c and T_4 for the SrF_2 and BaF_2 crystals are presented in figures 4 and 5. Figure 4 also shows the change of the 10 358 cm^{-1} line intensity with respect to the 10 361 cm^{-1} line intensity, depending on the Yb^{3+} ion concentration. The concentration dependence of the intensity ratio of optical lines with frequencies of 10 358 and 10 361 cm^{-1} is close to that for the EPR intensity ratio of T_c and T_4. From this fact we can conclude that the 10 358 cm^{-1} line corresponds to the 3^c transition for T_c, while the 10 361 cm^{-1} line corresponds to the 4^t transition for T_4. In the region of 10 340 cm^{-1} only one line is observed in the luminescence

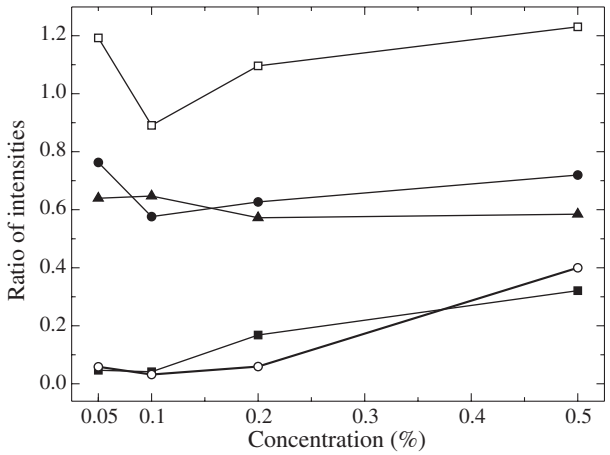

Figure 4. Concentration dependences of the ratios of the Yb^{3+} EPR intensities for T_c and T_4 in SrF_2 (○) and of those of the excitation luminescence intensities of lines with the frequencies: 10 358 and 10 361 cm^{-1} (■), 10 792 and 10 804 cm^{-1} (●), 10 792 and 10 814 cm^{-1} (□) and 10 814 and 10 804 cm^{-1} (▲).

excitation and luminescence spectra of the BaF_2:Yb^{3+} crystal. However, the shape of this line in the samples with a Yb^{3+} ion concentration of 0.01 and 0.2% makes it possible to suppose that this line consists of two unresolved components. If a xenon lamp is used as a source of luminescence excitation, then the sensitivity of our spectrometer does not allow measurements of the excitation luminescence spectra with a resolution higher than 3 cm^{-1}. As MCD in some cases has a higher resolution, the MCD spectrum in the region of 10 340 cm^{-1} was measured. The MCD spectrum for the BaF_2:Yb^{3+} crystal ($c = 0.2\%$) at $H = 300$ mT is presented in the inset to figure 3. In the MCD spectrum two components of the line were resolved and the distance between them is about 2 cm^{-1}. Figure 5 shows the numerical approximation of the luminescence excitation line at 10 340 cm^{-1} on the basis of two Voight's profiles with frequencies of 10 339 and 10 341 cm^{-1} for various concentrations of the Yb^{3+} ion. This approximation is given as a ratio of the line intensity with frequency 10 339 cm^{-1} to that with frequency 10 341 cm^{-1}. The comparison with the EPR data enabled us to conclude that the 10 339 cm^{-1} line corresponds to the 3^c transition for T_c, while the 10 341 cm^{-1} line corresponds to the 4^t transition for T_4. The numerical approximation of the group of the 10 780–10 820 cm^{-1} lines for SrF_2 and 10 720–10 790 cm^{-1} lines for BaF_2 is made in a similar way.

Figures 4 and 5 show the ratios of the line intensities associated with T_c and T_4 for SrF_2 and BaF_2, respectively. The character of the presented dependences for SrF_2:Yb^{3+} crystals allows us to assume that the 10 803 and 10 813 cm^{-1} lines belong to T_4 (the 5^t and 6^t transitions, respectively), while the line with frequency 10 789 cm^{-1} corresponds to T_c. For the BaF_2 crystals within the 10 720–10 790 cm^{-1} region, only two lines of the luminescence excitation were observed. The analysis of the dependences given in figure 2 shows that the 10 739 cm^{-1} line of the luminescence excitation belongs to T_c (the 4^c transition) and the 10 757 cm^{-1} line belongs to T_4 (the 6^t transition). The line of the luminescence excitation, corresponding to the 5^t transition, most probably coincides with the frequency of the 4^c transition or is close to it. This is supported by the fact that the line of luminescence excitation with frequency 10 739 cm^{-1} is also observed at a very low relative concentration of T_c, for example, for the BaF_2:Yb^{3+} crystal, $c = 0.05\%$. To confirm these results, attempts were made to redistribute the

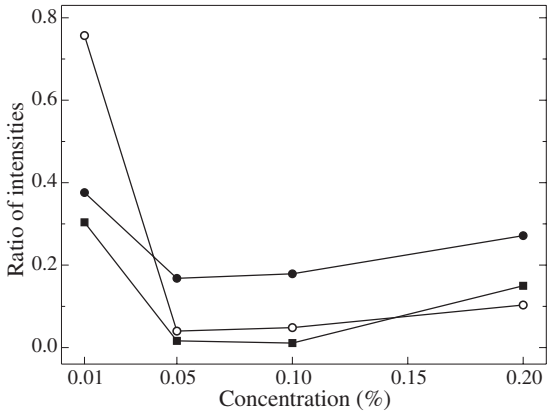

Figure 5. Concentration dependences of the ratios of the Yb^{3+} EPR intensities for T_c and T_4 in BaF_2 (○) and of those of the luminescence excitation intensities of lines with the frequencies: 10 339 and 10 341 cm^{-1} (■) and 10 742 and 10 758 cm^{-1} (●).

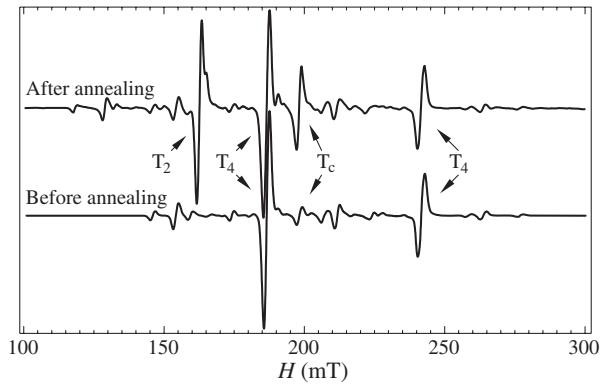

Figure 6. EPR spectra in SrF_2:Yb^{3+}($c = 0.2\%$) before and after annealing. $\boldsymbol{H} \parallel [111]$, $\nu = 9.35$ GHz, $T = 4.2$ K.

relative concentrations of PCs of cubic and trigonal symmetries. To this end, the samples were annealed (i.e. they were heated up to 850 °C in air for several hours and then they were quickly cooled to room temperature). Another stable PC, T_2, was formed in all samples. Considerable redistribution of the T_c and T_4 relative concentrations were observed in the SrF_2:Yb^{3+} crystal. Its EPR spectra before and after annealing are presented in figure 6. Spectra fragments of the luminescence excitation in the SrF_2:Yb^{3+} crystal before and after the annealing are shown in figure 7. The change of the relative intensities of the luminescence excitation lines, as a result of the redistribution of the T_c and T_4 relative concentrations, confirms the assumption that the luminescence excitation line with frequency 10 789 cm^{-1} corresponds to T_c, while the lines with frequencies 10 803 and 10 813 cm^{-1} belong to T_4.

As shown in energy level diagram (see the inset to figure 1), two luminescence lines belonging to T_c and three belonging to T_4 should be observed in luminescence spectra apart from the lines corresponding to the 3^c and 4^c transitions. In fact, in all samples one can observe only three intensive lines. Since these lines remain sufficiently intensive in the samples with the lowest relative concentration of T_c as well (according to EPR data), they should be attributed

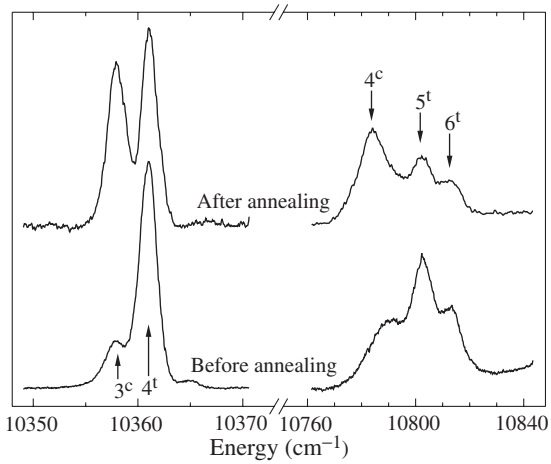

Figure 7. Fragments of the luminescence excitation spectra in SrF_2:Yb^{3+} ($c = 0.2\%$) at $T = 2$ K before and after annealing.

to the 1^t, 2^t and 3^t transitions for T_4. On the basis of the interpretation of the excitation luminescence spectra one can see that, as the crystal field symmetry lowers from cubic to trigonal, the splits of the quartet into $^2\Gamma_5$ and $^2\Gamma_4$ are small enough. This observation agrees well with the fact that, in the case of T_4, the additional ion, F^-, located at the nearest free cell along the C_3 axis, i.e. far enough away from the Yb^{3+} ion, is a compensator for the excess positive charge. Therefore, the distortions of the cube surrounding the Yb^{3+} ion should be not large. Therefore one can assume that in the T_4 ground multiplet, the positions of the $^1\Gamma_4$ and $^3\Gamma_4$ levels should not differ very much from the locations of the Γ_6 and Γ_8 levels, respectively, for T_c. In other words, the positions of the 1^c and 2^c luminescence lines may coincide or be close in frequency to the positions of the 1^t and 3^t lines, respectively. In the annealed SrF_2:Yb^{3+} crystal ($c = 0.2\%$) one observes a broadening and a small shift (of the order of 1 cm^{-1}) of the line, corresponding to the 3^t transition in the luminescence spectrum. From this, one may assume that the luminescence line associated with the 2^c transition is about 1 cm^{-1} lower in frequency with respect to the line associated with the 3^t transition. In the BaF_2:Yb^{3+} crystal ($c = 0.01\%$) with the largest relative concentration of PCs of the cubic symmetry, a weak luminescence line is also observed with a frequency of 9804 cm^{-1} which can be attributed to the 2^c transition. However, the lines, corresponding to the 1^c transition ($^2\Gamma_7 \rightarrow \Gamma_6$), were not registered in either the SrF_2 or BaF_2 crystals at the xenon lamp excitation of the luminescence. This is not surprising. This line has to be of low intensity because, due to the magnetic (or electric) dipole nature of the transitions, this line is forbidden according to the selection rules. The absence of such a luminescence line was also noticed in the CaF_2:Yb^{3+} crystal [4, 9]. Its observation in the PbF_2:Yb^{3+} crystal is probably due to the enhancement of the electron–lattice interaction in the PbF_2 compared to the complexes under consideration [5]. To detect the luminescence lines belonging to the transition 1^c and to confirm the interpretation of transitions 2^c in BaF_2:Yb^{3+} and SrF_2:Yb^{3+}, an experiment on LSE luminescence was carried out. The fragments of the LSE luminescence spectra in the BaF_2:Yb^{3+} and SrF_2:Yb^{3+} crystals of the 3^c and 4^t transitions are given in figures 8 and 9. In the BaF_2:Yb^{3+} crystal at LSE of the 3^c transition, two luminescence lines with frequencies 9796 and 9816 cm^{-1} were observed in addition to the 2^c transition identified previously. The first line can be attributed to the 1^c transition. The second line is evidence for the probable presence in the crystal of another

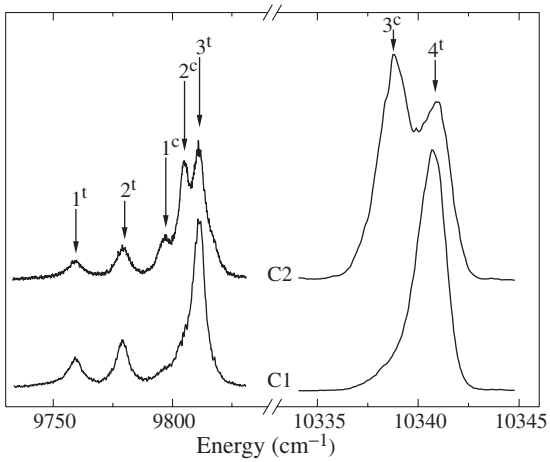

Figure 8. Fragments of the luminescence spectra in BaF_2:Yb^{3+}($c = 0.01\%$) with LSE at the frequencies 10 341 cm^{-1} (C1) and 10 339 cm^{-1} (C2) at $T = 2$ K.

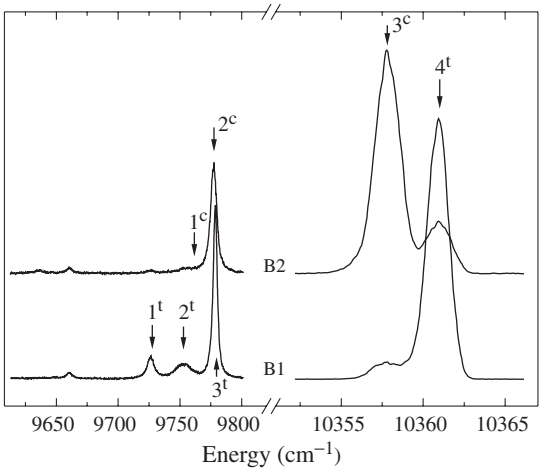

Figure 9. Fragments of the luminescence spectra in SrF_2:Yb^{3+}($c = 0.2\%$) with LSE at the frequencies of 10 361 cm^{-1} (B1) and 10 358 cm^{-1} (B2) at $T = 2$ K.

PC with concentration too small to be registered by EPR. The frequency of the transition from lowest level of the excited multiplet to the ground state of this PC is very close to the frequency of the 3^c transition. In the SrF_2:Yb^{3+} crystal at the LSE of the 3^c transition a weak luminescence line with a frequency of 9758 cm^{-1} was observed in addition to the 2^c transition. This line can be attributed to the 1^c transition. However, the weak intensity of this line in SrF_2 and the presence of the additional line in BaF_2, mentioned above, lead to ambiguity in the interpretation of the 1^c transitions. Therefore, in the further theoretical interpretation of the experimental results we will consider two variants. The first variant (I) corresponds to the case when these luminescence lines were not taken into consideration, i.e. the 1^c transition remains undetermined. In the second variant (II), the luminescence lines with the frequencies 9758 cm^{-1} for the SrF_2 and 9796 cm^{-1} for the BaF_2 crystals are attributed to the 1^c transition. Experimental results for the complexes under consideration are given in tables 1–3.

Table 2. Energy levels (in cm^{-1}) and g-factors of T_c in SrF_2 and BaF_2.

		SrF_2				BaF_2			
	Symmetry and	Experiment		Theory		Experiment		Theory	
J	g-factors	I	II	I	II	I	II	I	II
5/2	$^2\Gamma_8$	10 783	10 783	10 783	10 783	10 739	10 739	10 739	10 737
	$^2\Gamma_7$	10 358	10 358	10 358	10 370	10 339	10 339	10 339	10 356
7/2	Γ_6		600	625	607		542	585	556
	$^1\Gamma_8$	586	586	586	584	535	535	535	539
	$^1\Gamma_7$	0		0		0		0	
	$g(^1\Gamma_7)$	|3.441|		3.479	3.480	|3.422|		3.476	3.477

Table 3. Energy levels (in cm^{-1}) and g-factors of T_4 in SrF_2 and BaF_2.

		SrF_2		BaF_2	
	Symmetry and				
J	g-factors	Experiment	Theory	Experiment	Theory
5/2	$^5\Gamma_4$	10 813	10 814	10 757	10 757
	$^2\Gamma_{56}$	10 802	10 802	10 739	10 739
	$^4\Gamma_4$	10 361	10 370	10 341	10 345
7/2	$^3\Gamma_4$	635	642	582	585
	$^2\Gamma_4$	608	611	562	564
	$^1\Gamma_{56}$	583	586	530	531
	$^1\Gamma_4$	0	0	0	0
	$g_\parallel(^1\Gamma_4)$	|2.811|	2.811	|2.763|	2.771
	$g_\perp(^1\Gamma_4)$	|3.743|	−3.807	|3.768|	−3.820

3. Analysis of the crystal field parameters and the estimation of the lattice local distortions

3.1. Determining the potentials of crystal fields

To interpret the experimental values of the energy levels and g-factors presented in tables 2 and 3, the energy matrix, considering the spin–orbit interaction and the interaction with a crystal field, for the Yb^{3+} crystal (configuration $4f^{13}$, term ^2F), was formed. The Hamiltonian of the spin–orbit interaction was used in the form $H_{so} = -\xi(\boldsymbol{SL})$ where ξ is the spin–orbit interaction parameter and $\boldsymbol{S}$ and $\boldsymbol{L}$ are the operators of the spin and orbital moment of the Yb^{3+} ion, respectively. The interaction of the Yb^{3+} ion with the crystal field for the PC of T_c was described by the Hamiltonian $H_{cr}(O_h) = B_4(V_4^0+5V_4^4)+B_6(V_6^0-21V_6^4)$, where the Descartes coordinates of the 4f-electrons in harmonic polynomials V_k^q [10] were related to the cubic axes of the crystal. The Hamiltonian for T_4 has the form: $H_{cr}(C_{3v}) = B_2^0V_2^0+B_4^0V_4^0+B_4^3V_4^3+B_6^0V_6^0+B_6^3V_6^3+B_6^3V_6^3$. In order to fix the signs of the B_4^3 and B_6^3 parameters, the axis z of the system of coordinates used was matched to the symmetry axis of the centre. The two other axes were directed in such a way that one of the fluorine ions in the near vicinity was in the positive quadrant of the zOx plane. (The location of the T_4 axes with respect to the cubic axes corresponded to that of Watanabe [11].) From the diagonalization of the matrix of the Hamiltonian $H_{so}+H_{cr}$, the theoretical energy levels and wavefunctions were determined. The wavefunctions of the ground-state Kramers doublet were used then to calculate the g-factors of the spin

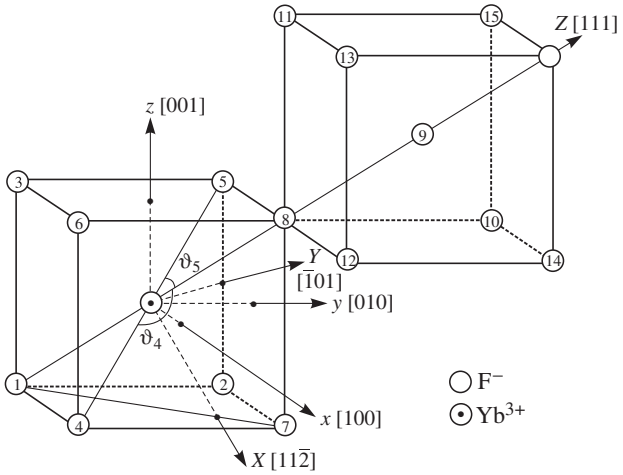

Figure 10. Deformation structural model of T_4.

Hamiltonian $\beta \boldsymbol{H} g \boldsymbol{S}'$, where $\boldsymbol{H}$ is the magnetic field strength and $\boldsymbol{S}'$ is the effective $S' = 1/2$ spin operator of the Yb^{3+} ion. Matrix elements of the Zeeman interaction Hamiltonian $H_z = \beta \boldsymbol{H}(\boldsymbol{L} + g_s \boldsymbol{S})$, where β is the Bohr magneton and $g_s = 2.002\,32$ is the g-factor of a free electron, diagonal with respect to total moment J, were calculated taking into account the Lande g-factors of the corresponding multiplets ($g_{7/2} = 6/7 + g_s/7$, $g_{5/2} = 8/7 - g_s/7$). The off-diagonal matrix elements were found by the Wigner–Eckart theorem with the reduced element $(^2F_{7/2} \parallel L + g_s \boldsymbol{S} \parallel {}^2F_{5/2}) = 4(g_s - 1)\sqrt{3/14}$. Then five theoretical quantities for T_c (the g-factor and four energy differences) and eight quantities for T_4 (two g-factors and six energy differences) were least-squares fitted to the corresponding experimental values to find the best-fit values of g-factors, crystal field and spin–orbit interaction parameters [12]. Tables 2–5 give the results of approximation. The maximal standard deviation of the theoretical values of the energy levels from the experimental ones is less than 13 cm^{-1}. The values of the g-factors of T_4 are described well enough, however, the differences of the theoretical g-factors from their experimental values for T_c the same as in the PbF_2:Yb^{3+} crystal [5], were considerably larger than the experimental error. The weak anisotropy of the g-factors of T_4 shows that its crystal field does not differ very much from that of T_c (table 5).

The $g_\parallel$ and $g_\perp$ values of T_4 agree very well with the fact that the doublet, originating from the doublet $^1\Gamma_7$ of T_c, is the lowest Kramers doublet. However, it should be kept in mind when calculating the mean g-factor of this doublet $\tilde{g}$ that, at the transition of the wavefunctions of the Γ_7 representation of the O_h group into the wavefunctions of the Γ_4 representation of the C_{3v} group, the functions change places and one of them changes sign. So, for the $\tilde{g}$ of the T_4, for example, in SrF_2, we will have $\tilde{g} = [g_\parallel + 2(-g_\perp)]/3 = 3.476$. The crystal field parameters for T_c in the SrF_2 and BaF_2 crystals agree both in the sign and value with the parameters of the similar centres in the CaF_2 [9] and PbF_2 [5] crystals and follow the general tendency to decrease as the lattice constant a_0 increases. Potentials of T_c in the SrF_2 and BaF_2 crystals also agree well with each other.

3.2. Structure of T_4

Table 5 shows that the crystal field parameters for T_4 and T_c^{trig} in SrF_2 and BaF_2 crystals are very close to each other. The crystal field on the paramagnetic ion is determined mainly by

the electrostatic and contact interactions of the Yb^{3+} ion with the nearest fluorine ions. Due to this fact, one can suppose that when the T_4 is formed, the positions of F^- ions are essentially the same as those they occupied in T_c. Investigations of such centres in SrF_2 and BaF_2 crystals by the radio-frequency discrete saturation method (see, e.g., [13] and [14], respectively) show that only the ^{19}F nuclei, located close to the ion-compensator (F_9) are notably shifted, and that the vicinity of the Yb^{3+} ion can be separated into two regions (figure 10). In the first region (not containing F_9) the positions of the fluorine ions of the first (F_1–F_4) and distant coordinate spheres do not practically differ from their coordinates in the T_c. In the second region (containing F_9), the fluorine ions of the first (F_5–F_8), second (F_{10}–F_{12}) and third (F_{13}–F_{15}) coordinate spheres, and the ion-compensator F_9 are shifted. To estimate the quantitative lattice crystal distortion near the impurity ion, the superposition model (SM) [15–17] was used on the basis of the obtained qualitative structure of the T_4 complexes of the Yb^{3+} ion. This model postulates that the total crystal field is the linear superposition of the fields generated by each crystal ion. The resultant parameters of the crystal field are presented then in the form:

$$B_k^q = \sum_i K_k^q(\vartheta_i, \phi_i)\bar{B}_k(R_i), \tag{1}$$

where $K_k^q(\vartheta_i, \phi_i)$ are the structure factors depending on the angular positions (determined by the spherical angles ϑ_i and ϕ_i) of all ions located at a distance R_i from the paramagnetic ion (the most complete table of their expressions is given in [18]); $\bar{B}_k(R_i)$ are the intrinsic parameters depending on the type of ligands. In practice, it is usually assumed that the dependence of the $\bar{B}_k(R_i)$ parameters on R_i obeys the following law in a limited range of distances:

$$\bar{B}_k(R_i) = \bar{B}_k(R_0)\left(\frac{R_0}{R_i}\right)^{t_k}, \tag{2}$$

where t_k is a power and $\bar{B}_k(R_0)$ is the intrinsic model parameter corresponding to a certain mean distance R_0, usually assumed to be equal to the sum of the ion radii of the magnetic ion and ligand. If the equilibrium positions of F^- with respect to the Yb^{3+} impurity ions are specified, then the values of t_k and $\bar{B}_k(R_0)$ can be determined from the parameters of the crystal field of the T_c in a series of the CaF_2, SrF_2 and BaF_2 isomorphic crystals. These parameters are shown in table 4. Distances to the nearest neighbours (R_{Yb-F}) can be obtained either empirically by measuring the A_s and A_p parameters of the ligand hyperfine structure and assuming that they follow certain exponential laws similar to (2) [19–21], or by the theoretical calculations, minimizing the energy of this or that lattice complex including the centre under consideration, as in [22–24]. The A_s and A_p parameters of T_c in fluorites [24] are not specified correctly enough to use, for example, the procedure [21] for determining R_{Yb-F} (the method, suggested in [19], does not give the linear dependences for this case). Therefore, it seems reasonable to use theoretical data of [23] to determine the values of R_{Yb-F}, since the results of this work for the Eu^{2+}, Gd^{3+} and Tm^{2+} ions agree very well with the calculations carried out in [25] for the same ions in a more strict model.

Let us assume that the crystal field in cubic centres is formed only by the eight nearest ions of F^- and that the R_1 distances from the Yb^{3+} ion to these ions in CaF_2, SrF_2 and BaF_2 are equal to 2.2907, 2.3194 and 2.3478 Å, respectively [24]. Then, for the intrinsic parameters of the 4th- and 6th-order (in cm^{-1}) for variant I we will have: $\bar{B}_4(R_1) \rightarrow 68.75, 62.76, 58.68$; $\bar{B}_6(R_1) \rightarrow 19.03, 17.12, 14.90$. Logarithmic dependences of the numerical values of these parameters as the logarithmic functions of numerical values of the R_1 distances, are well extrapolated by the straight lines, their inclinations giving the values $t_4 = 6.4 \pm 0.5$ and $t_6 = 9.9 \pm 0.9$ for the powers in (2). It should be noted that the values t_4 and t_6 are very close to $t_4 = 6.3 \pm 1.4$ and $t_6 = 10.1 \pm 1.1$ for the Er^{2+}, Dy^{3+} and Tb^{2+} ions in the

Table 4. Parameters (in cm^{-1}) of crystal field (B_4, B_6) and the spin–orbit interaction (ξ) for T_c in MeF_2.

	Lattice constant	ξ		B_4		B_6	
Crystal	a_0 (Å) [20]	I	II	I	II	I	II
CaF_2 [4, 9]	5.443	2908.9		−213.9		33.8	
SrF_2	5.780	2908.4	2911.2	−195.3	−190.2	30.4	31.9
β-PbF_2 [5]	5.901	2907.3		−196.0		24.8	
BaF_2	6.178	2909.0	2911.5	−182.6	−175.1	26.5	30.0

same crystals [16]. Then, taking the sum of ion radii of the Yb^{3+} and F^- ions to be equal to $R_0 = 2.295$ Å [26], we find the intrinsic parameters of the model from the equation of straight lines $\bar{B}_4(R_0) = \bar{B}_4 = 67.7 \pm 2.4\ cm^{-1}$ and $\bar{B}_6(R_0) = \bar{B}_6 = 18.8 \pm 4.1\ cm^{-1}$.

In the nearest surrounding cube, the F_1, F_2, F_3 and F_4 ions take up positions with the coordinates $R_1 = R_2 = R_3 = R_4$, $\vartheta_1 = 0$, $\vartheta_2 = \vartheta_3 = \vartheta_4 = 109.47°$ ($\sin\vartheta/2 = \sqrt{2/3}$, $\cos\vartheta/2 = \sqrt{1/3}$), $\phi_2 = 60°$, $\phi_3 = 180°$, $\phi_4 = 300°$ in the system of coordinates of T_4, while the coordinates of the next four F_5, F_6, F_7 and F_8 ions, are as follows: $R_5 = R_6 = R_7 = R_8 = R_1$, $\vartheta_5 = \vartheta_6 = \vartheta_7 = 70.53°$ ($\sin\vartheta/2 = \sqrt{1/3}$, $\cos\vartheta/2 = \sqrt{2/3}$), $\vartheta_8 = 0$, $\phi_5 = 120°$, $\phi_6 = 240°$, $\phi_7 = 0$. In the analysis given below, it is supposed that when T_4 is formed, the R_5 and ϑ_5 coordinates of the F_5, F_6, F_7 ions, as well as the R_8 distance to the axial F_8 ion, change. Within the frame of the SM, one more term is added to the expression (1) in summation with respect to i, due to the appearance of the F_9 ion-compensator located at the R_9 distance from the Yb^{3+} ion. The changes of the crystal field parameters $\Delta B_k^q = B_k^q(T_4) - B_k^q(T_c^{trig})$, taking place in this case, are described by the following system of equations:

$$\begin{aligned}
\Delta B_4^0 &= 3\bar{B}_4(R_5)K_4^0(\vartheta_5) + \bar{B}_4(R_8) + \bar{B}_4(R_9) - \tfrac{28}{27}\bar{B}_4(R_1)\\
\Delta B_4^3 &= 3\bar{B}_4(R_5)K_4^3(\vartheta_5) - \frac{560\sqrt{2}}{27}\bar{B}_4(R_1)\\
\Delta B_6^0 &= 3\bar{B}_6(R_5)K_6^0(\vartheta_5) + \bar{B}_6(R_8) + \bar{B}_6(R_9) - \tfrac{128}{81}\bar{B}_6(R_1)\\
\Delta B_6^3 &= 3\bar{B}_6(R_5)K_6^3(\vartheta_5) + \frac{1120\sqrt{2}}{81}\bar{B}_6(R_1)\\
\Delta B_6^6 &= 3\bar{B}_6(R_5)K_6^6(\vartheta_5) - \tfrac{1232}{81}\bar{B}_6(R_1).
\end{aligned} \tag{3}$$

From this system, taking into account the values of ΔB_k^q, given in table 5, one can obtain, in principle, the R_5, ϑ_5, R_8 and R_9 parameters, characterizing the structure of T_4. In the potential of T_4, the B_2^0 parameter also appears, which was absent in T_c. However, the use of the equation for that parameter would lead one beyond the frame of the ligand SM [15, 16]. (A substantial contribution to the value of the B_2^0 parameter means that the magnetic ion interacts (mainly electrostatically) with the more distant ions of the lattice and not only with the nearest nine F^- ions under consideration.) We may assume, that the dependences (2) for the $\bar{B}_4(R_8)$ and $\bar{B}_6(R_8)$ parameters in the system (3) will be valid, with the same t_4 and t_6 powers and $\bar{B}_4(R_0)$ and $\bar{B}_6(R_0)$ intrinsic parameters as for the values of $\bar{B}_4(R_5)$ and $\bar{B}_6(R_5)$. However, for the values of $\bar{B}_4(R_9)$ and $\bar{B}_6(R_9)$, the set of corresponding parameters will be, naturally, different, due to the R_9 distance to the ion-compensator being almost twice as much as R_8. At such distances the contact interactions, caused by the covalence and overlap of the electron shells, considerably decay and the pure electrostatic effects will become quite important. These effects lead to the change in the sign of the $\bar{B}_4(R_9)$ and $\bar{B}_6(R_9)$ values at

the certain R_9 distances. In this case, in the frame of the ligand SM, the $\bar{B}_4(R_9)$ and $\bar{B}_6(R_9)$ values cannot be obtained in principle, since the intrinsic parameters and the structure factors for the F_9 ion are positive. Therefore, the system (3) can be solved under the assumption that the $\bar{B}_4(R_9)$ and $\bar{B}_6(R_9)$ values are the unknown parameters of the theory. Writing the system in the form

$$\begin{aligned}
&3\bar{B}_4\left(\frac{2.295}{R_5}\right)^{6.4} 35\sin^3\vartheta_5\cos\vartheta_5 - \frac{560\sqrt{2}}{27}\bar{B}_4(R_1) - \Delta B_4^3 = 0\\
&3\bar{B}_6\left(\frac{2.295}{R_5}\right)^{9.9} \frac{105}{8}\sin^3\vartheta_5\cos\vartheta_5(11\cos^2\vartheta_5 - 3) + \frac{1120\sqrt{2}}{81}\bar{B}_6(R_1) - \Delta B_6^3 = 0\\
&3\bar{B}_6\left(\frac{2.295}{R_5}\right)^{9.9} \frac{231}{32}\sin^6\vartheta_5 - \frac{1232}{81}\bar{B}_6(R_1) - \Delta B_6^6 = 0\\
&\frac{3}{8}\bar{B}_4\left(\frac{2.295}{R_5}\right)^{6.4} (35\cos^4\vartheta_5 - 30\cos^2\vartheta_5 + 3) + \bar{B}_4\left(\frac{2.295}{R_8}\right)^{6.4}\\
&\qquad - \tfrac{28}{27}\bar{B}_4(R_1) + \bar{B}_4(R_9) - \Delta B_4^0 = 0\\
&\frac{3}{16}\bar{B}_6\left(\frac{2.295}{R_5}\right)^{9.9} (231\cos^6\vartheta_5 - 315\cos^4\vartheta_5 + 105\cos^2\vartheta_5 - 5) + \bar{B}_6\left(\frac{2.295}{R_8}\right)^{9.9}\\
&\qquad - \tfrac{128}{81}\bar{B}_6(R_1) + \bar{B}_6(R_9) - \Delta B_6^0 = 0
\end{aligned} \tag{4}$$

one can use it to find five quantities: R_5, ϑ_5, R_8, $\bar{B}_4(R_9)$ and $\bar{B}_6(R_9)$. As our estimations show (carried out in a point approximation), the absolute values of the $\bar{B}_4(R_9)$ and $\bar{B}_6(R_9)$ parameters are small and cannot exceed several cm^{-1}. Taking this into account, we obtain by solving the system (4) for the SrF_2: $R_5 = 2.36 \pm 0.03$ Å, $\vartheta_5 = 67 \pm 4°$, $R_8 = 2.21 \pm 0.04$ Å, $\bar{B}_4(R_9) = -0.8$ cm^{-1}, $\bar{B}_6(R_9) = -0.02$ cm^{-1} and for the BaF_2: $R_5 = 2.38 \pm 0.05$ Å, $\vartheta_5 = 69 \pm 5°$, $R_8 = 2.28 \pm 0.06$ Å, $\bar{B}_4(R_9) = -0.6$ cm^{-1}, $\bar{B}_6(R_9) = -0.02$ cm^{-1}. A comparison of R_5, ϑ_5, R_8 values with the coordinates in undoped crystals (2.503 Å, 70.53°, 2.503 Å [23] and 2.675 Å, 70.53°, 2.675 Å [24]) shows that three fluorine ions from the nearest surrounding cube, located symmetrically with respect to the C_3 axis from the side of the ion-compensator, approach the impurity ion and cling to the axis of the centre when T_4 is formed in the SrF_2 and BaF_2 crystals. In SrF_2, lattice angular distortions are more substantial. It should be noted, however, that the clinging of the fluorine ions to the axis of the centre is not strict, since an inaccuracy of the $\vartheta_5(\Delta\vartheta_5 \sim 5°)$ angles calculated exceeds the obtained change of these angles ($\Delta \sim 3°$) when T_4 is formed. The R_8 distances obtained demonstrate a considerable movement of the F_8 axial ion towards the Yb^{3+} impurity ion. Theoretical values of the B_4^0, B_4^3, B_6^0, B_6^3 and B_6^6 crystal field parameters on the basis of the R_5, ϑ_5, R_8, $\bar{B}_4(R_9)$ and $\bar{B}_6(R_9)$ values obtained for T_4 are given in table 5 in lines 'T_4(SM) I'. It is shown that the differences between the theoretical values and experimental ones are not so large and the 4th-order parameters are described very well.

If we repeat all the calculations, taking parameters II as the initial parameters of the crystal field, we have for the intrinsic parameters of the 4th- and 6th-order (in cm^{-1}): $\bar{B}_4(R_1) \to 68.75, 61.15, 56.27$; $\bar{B}_6(R_1) \to 19.03, 17.97, 16.94$. For the powers in equation (2) we find $t_4 = 8.2 \pm 0.8$ and $t_6 = 4.7 \pm 0.1$, which differ strongly from those in [16] and parameters I. Moreover, $t_6 < t_4$, which contradicts the point model of the crystal field predicting $t_6 > t_4$. This situation took place previously in [27] in which the SM was used to interpret the crystal field parameters of all series of the rare-earth trivalent ions in $LaCl_3$:Ln^{3+} and Cs_2NaYCl_3:Ln^{3+}. The following values for the model intrinsic parameters were obtained: $\bar{B}_4(R_0) = \bar{B}_4 = 67.4 \pm 3.5$ cm^{-1} and $\bar{B}_6(R_0) = \bar{B}_6 = 18.9 \pm 1.1$ cm^{-1}. The solution of the system (3) for the SrF_2 crystal gives: $R_5 = 2.36 \pm 0.02$ Å, $\vartheta_5 = 66 \pm 1°$, $R_8 = 2.20 \pm 0.03$ Å, $\bar{B}_4(R_9) = -0.8$ cm^{-1}, $\bar{B}_6(R_9) = -0.02$ cm^{-1} and for the BaF_2: $R_5 = 2.39 \pm 0.02$ Å,

Table 5. Parameters (in cm^{-1}) of the crystal field (B_k^q) and the spin–orbit interaction (ξ) for T_c and T_4 in SrF_2 and BaF_2. $\Delta B_k^q = B_k^q(T_4) - B_k^q(T_c^{trig})$ where T_c^{trig} denotes cubic parameters in the trigonal axes.

Crystal			ξ	B_2^0	B_4^0	B_4^3	B_6^0	B_6^3	B_6^6
SrF_2	T_4		2911.2	101	139	3644	64	−551	487
	T_4(SM)	I			139	3645	67	−570	453
	T_c^{trig}		2908.4	0	130	3682	54	−670	521
	ΔB_k^q			101	9	−38	10	119	−34
	T_4(SM)	II			138	3536	66	−587	480
	T_c^{trig}		2911.2	0	126	3586	57	−703	547
	ΔB_k^q			100	13	58	7	152	−60
BaF_2	T_4		2909.5	101	125	3347	58	−515	449
	T_4 (SM)	I			128	3348	53	−536	418
	T_c^{trig}		2909.0	0	122	3443	47	−583	453
	ΔB_k^q			101	3	−96	11	68	−4
	T_4 (SM)	II			126	3256	64	−521	441
	T_c^{trig}		2911.4	0	117	3301	53	−660	514
	ΔB_k^q			101	8	46	5	145	−65

$\vartheta_5 = 65 \pm 1°$, $R_8 = 2.21 \pm 0.03$ Å, $\bar{B}_4(R_9) = -0.7$ cm^{-1}, $\bar{B}_6(R_9) = -0.02$ cm^{-1}. The picture of deformations in the vicinity of the paramagnetic ion in II is qualitatively the same as in I. The clinging of the fluorine ion at the axis of the centre in II is undoubted since the inaccuracy in the angle values, ϑ_5, does not exceed 1°. Theoretical values of the B_4^0, B_4^3, B_6^0, B_6^3 and B_6^6 crystal field parameters are given in table 5 in lines 'T_4(SM) II'. The differences between theoretical and experimental values are again not so large, however, in this case, unlike for parameters I, the 6th-order parameters are better described.

4. Conclusion

Crystals of the fluorine homological series (SrF_2 and BaF_2), doped with the ytterbium ions, forming T_c and T_4 were investigated by EPR and optical spectroscopy. To increase the reliability in the interpretation of the Yb^{3+} optical spectra, crystals with different concentrations of ytterbium, crystal annealing and also the LSE technique were used. A weak intensity of one of the optical transition in T_c led to ambiguity in the interpretation of the potential of the crystal field of the cubic symmetry. To estimate the crystal lattice distortion near the Yb^{3+} impurity ion for T_4, a SM was applied. Both variants of the potential of the crystal field of the cubic symmetry resulted in the same picture of deformations surrounding the paramagnetic ion. When T_4 is formed, three fluorine ions from the first coordinate sphere (F_5–F_7) approach the impurity ion and cling to the axis of the centre. The fluorine ion, located at the PC axis between the Yb^{3+} ion and the ion-compensator (F_9), approach close to the impurity ion as well. This structural model of T_4 does not agree with the results presented in [28, 29] for the analogous PC of the Gd^{3+} ion in BaF_2 crystal.

Acknowledgment

This work was supported by the Russian Foundation for Basic Research (project No 02–02–16648).

References

[1] Ranon A and Yaniv U 1964 *Phys. Lett.* **9** 17–19
[2] Berulava B G, Mirianashvili P I, Nazarova O V and Sanadze T I 1977 *Fiz. Tverd. Tela* **19** 1771–4
[3] Kirton J and White A M 1969 *Phys. Rev.* **178** 543–7
[4] Anderson C H 1974 *Crystal With the Fluorite Structure* ed W Hayes (Oxford: Clarendon) ch 5
Baker J M 1974 *Crystal With the Fluorite Structure* ed W Hayes (Oxford: Clarendon) ch 6
[5] Gerasimov K I, Leushin A M and Falin M L 2001 *Phys. Solid State* **43** 1675–9
[6] Falin M L, Gerasimov K I, Leushin A M, Bill H, Lovy D and Sanadze T 2001 *J. Alloys Compounds* **323/324** 692–5
[7] Latypov V A and Falin M L 2001 *Prib. Tehn. Eksp.* **4** 164–6 (in Russian)
[8] Falin M L, Gerasimov K I, Kazakov B N and Yakshin M A 1999 *Appl. Magn. Reson.* **17** 103–12
[9] Kiro D and Low W 1970 *Magnetic Resonance* ed C K Coogan, N S Ham, S N Stuart, J R Pilbrow and G V H Wilson (New York: Plenum) pp 247–69
[10] Stevens K W H 1952 *Proc. Phys. Soc.* A **65** 209
[11] Rudowicz C 1987 *Magn. Reson. Rev.* **13** 1–89
[12] Pearson J J, Herrman G F, Wickersheim K A and Buchanan R A 1967 *Phys. Rev.* **159** 251–61
[13] Nazarova O V and Sanadze T I 1978 *Fiz. Tverd. Tela* **20** 620–2
[14] Nazarova O V and Sanadze T I 1977 *Bull. Acad. Sci. Georgian SSR, Phys.* **8** 329–32
[15] Newman D J 1971 *Adv. Phys.* **20** 197–256
[16] Newman D J 1978 *Aust. Phys.* **31** 79–93
[17] Newman D J 1980 *Aust. Phys.* **33** 733–43
[18] Rudowicz C 1987 *J. Phys. C: Solid State Phys.* **20** 6033–7
[19] Anderson C H, Call P, Stott J and Hayes W 1975 *Phys. Rev.* B **11** 3305–10
[20] Baker J M 1979 *J. Phys. C: Solid State Phys.* **12** 4039–49
[21] Falin M L, Meiklyar V P and Konkin A L 1980 *J. Phys. C: Solid State Phys.* **13** 1299–303
[22] Ivanenko Z I and Malkin B Z 1970 *Sov. Phys.–Solid State* **11** 1498–503
[23] Tovar M, Ramos C A and Fainstein C 1983 *Phys. Rev.* B **28** 4813–17
[24] Ramos C A, Fainstein C and Tovar M 1985 *Phys. Rev.* B **32** 64–8
[25] Yeung Y Y 1988 *J. Phys. C: Solid State Phys.* **21** L549–53
[26] Shannon R D 1976 *Acta Crystallogr.* B **32** 751–67
[27] Reid M F and Richardson F S 1985 *J. Chem. Phys.* **83** 3831–6
[28] Gorlov A D and Potapov A P 2000 *Phys. Solid State* **42** 51–4
[29] Gorlov A D, Guseva A D, Potapov A P and Rokeah A I 2001 *Phys. Solid State* **43** 473–9